Investigation on an application of silver substrates for sensitive surface plasmon resonance imaging detection

Seung Ho Choi[1] and Kyung Min Byun[2,*]

[1]*Interdisciplinary Program of Bioengineering, Seoul National University, Seoul 152-742, Korea*
[2]*Department of Biomedical Engineering, Kyung Hee University, Yongin 446-701, Korea*
[*]*Corresponding author: kmbyun@khu.ac.kr*

Received April 8, 2010; revised July 22, 2010; accepted August 20, 2010;
posted August 27, 2010 (Doc. ID 126754); published September 22, 2010

A surface plasmon resonance (SPR) imaging biosensor based on silver substrates was investigated to demonstrate that silver could be used as a substrate material for sensitive detection of biomolecular interactions, despite its poor chemical stability. The calculation results showed that oxidation of silver film may lead to a decrease in the sensitivity due to a variation in SPR characteristics such as a broader curve width and shallower minimum reflectance at resonance. The effect of a change in the refractive index of target analytes on the sensitivity was also explored. In particular, it is noteworthy that Ag/Au bimetallic substrates with a thin gold protection layer to prevent oxidation of a silver film can provide a significant amplification of SPR imaging signals in comparison with conventional gold substrates.

OCIS codes: 130.6010, 240.6680, 310.6845.

1. INTRODUCTION

The phenomenon of surface plasmon resonance (SPR) has evolved into a promising technique for biological analysis applications since it provides rapid, label-free, and quantitative sensing capability [1,2]. In principle, SPR characteristics are sensitive to environmental changes caused by an immobilization of biomolecules, and thus this technique has been employed to characterize bio-affinity interactions onto a thin metal film. Fluorescence-based biosensors have been developed quickly as well [3,4]; however, they require complicated processes of binding fluorescence tags and are afflicted with a lack of quantitative accuracy and photobleaching [5]. For this reason, surface-sensitive optical biosensing based on SPR is applied heavily to the detection of biochemical reactions, such as antigen/antibody, protein/protein, and deoxyribose nucleic acid (DNA) interactions [6].

In general, four detection methods have been used mainly as a SPR biosensor, involving wavelength interrogation, angle interrogation, phase measurement, and intensity measurement [7]. Recently, since development of a high-throughput system has been emerged as one of the most important SPR sensing applications with increasing demands for a rapid measure of a large number of samples, most of the relevant studies have employed an intensity-based detection scheme, called SPR imaging. This approach that measures reflectance changes induced by a slight variation in the refractive index on a sensor surface has drawn much interest due to the simplicity in structure without any moving parts and the adaptability to multi-channel configurations.

The sensitivity of a SPR imaging sensor is another important concern [8]. Currently, while silver films with a narrower SPR curve in the visible band yield higher sensitivity than gold films, they have never been widely used in SPR imaging biosensors because silver is known to be highly susceptible to oxidation. On the other hand, regardless of the advantage of gold films, which tend to be chemically stable, SPR imaging systems based on gold substrates suffer from relatively low detection accuracy arising from insufficient sensitivity. In other words, regarding stability and reliability considerations in actual experiments, although the use of a thin gold film might be a better choice, silver films would be potential candidates for practical SPR substrates if coated silver surfaces could be made chemically inert [9].

Therefore, in this paper, we theoretically consider a SPR imaging structure based on a thin silver film in order to improve the sensitivity of intensity measurements. First, since a silver oxide layer can be formed experimentally by reactive sputtering of pure silver in an oxygen-containing argon atmosphere or by thermal or electron-beam evaporation of pure silver followed by oxidation in an oxygen plasma [10], the effect of a silver oxide formation on the SPR imaging performance is investigated. Due to its nonzero imaginary dielectric constant, the growth of a silver oxide layer may produce extra damping of propagating surface plasmons, resulting in an increased SPR curve width. Second, the reflectance change also occurs from the resonance shift created by the changes in the refractive index at the sensor surface. It is thus an obvious next step to explore the influence of a concentration of bound analytes on the SPR imaging characteristics. Third, in order to overcome the drawbacks of silver oxide formation, an alternative structure of bimetallic Ag/Au surfaces, where a thin gold film is coated over the silver substrate, is proposed. Employing a bimetallic substrate enables one to eliminate the possibility of silver oxidation

and simultaneously to achieve optimal SPR imaging performance for eventual biosensing applications. As a result, from this study, we intend to demonstrate a viable potential for applying silver substrates to a sensitive detection of biomolecular interactions.

2. NUMERICAL MODEL

A schematic diagram of a SPR imaging system is shown in Fig. 1. Uniform silver films are deposited on a SF10 prism substrate via an attachment layer of chromium with a thickness fixed at $d_1=2$ nm. Note that, while the SPR platform in Fig. 1 is practically based on the Kretschmann configuration employing a prism coupler, the prism substrate in this theoretical study is defined as a semi-infinite dielectric medium. The initial thickness of the silver layer is 40 nm, and it is converted into a silver oxide (Ag_2O) layer under the atmospheric condition of an oxygen-containing plasma [11]. Binding analytes are modeled as a 1-nm-thick self-assembled monolayer (SAM), which covers the whole sensor surface. A transverse-magnetic (TM)-polarized light with $\lambda=633$ nm is used to illuminate the prism/thin silver film sample at a predetermined incidence angle that produces a maximal intensity change. The optical constants $\varepsilon=(n,k)$ of the SF10 prism substrate and thin layers of chromium, silver, and silver oxide were determined as (1.723,0), (3.48,4.36), (0.059,4.243), and (2.50,0.11), respectively, at $\lambda=633$ nm [12–14]. The refractive index of the water solution was assumed to be 1.33.

When a TM-polarized light is incident into the SPR imaging system at an angle θ as shown in Fig. 1, the analytical solution of reflectance R is represented by a 2×2 M-matrix, which is a serial product of the interface matrix I_{jk} ($j=0$, 1, 2, 3, 4, and $k=j+1$) and the layer matrix L_j as follows [15]:

$$R=\left|\frac{M_{12}}{M_{22}}\right|^2, \tag{1}$$

where

$$M=\begin{bmatrix}M_{11} & M_{12}\\ M_{21} & M_{22}\end{bmatrix}=I_{01}L_1I_{12}L_2I_{23}L_3I_{34}L_4I_{45}, \tag{2}$$

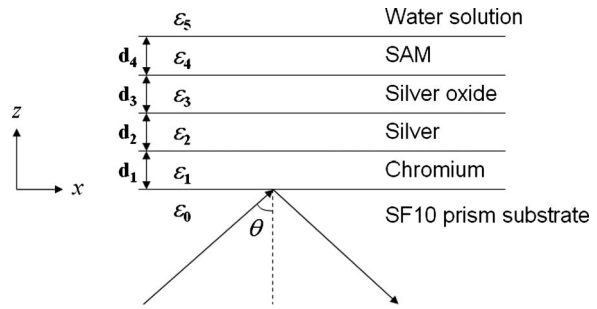

Fig. 1. Schematic diagram of a thin-film-based SPR configuration with a silver oxide coating. TM-polarized light with $\lambda=633$ nm propagating into a SF10 prism substrate is incident on an adhesion layer of chromium ($d_1=2$ nm), a thin silver film (d_2), and a silver oxide film (d_3) with an incidence angle of θ. Binding analytes are modeled as 1 nm thick SAM in water solution.

$$I_{jk}=\begin{bmatrix}1 & r_{jk}\\ r_{jk} & 1\end{bmatrix},\quad L_j=\begin{bmatrix}e^{ik_{zj}d_j} & 0\\ 0 & e^{-ik_{zj}d_j}\end{bmatrix}. \tag{3}$$

Here, r_{jk}, k_{zj}, and d_j represent the Fresnel reflection coefficient, the wave-vector in the z-direction, and the thickness of the jth layer, respectively. r_{jk} and k_{zj} are given by

$$r_{jk}=\frac{\left(\frac{k_{zj}}{\varepsilon_j}-\frac{k_{zk}}{\varepsilon_k}\right)}{\left(\frac{k_{zj}}{\varepsilon_j}+\frac{k_{zk}}{\varepsilon_k}\right)}, \tag{4}$$

$$k_{zj}=\sqrt{\varepsilon_j\left(\frac{\omega}{c}\right)^2-k_x^2},\quad \text{with}\quad k_x=\sqrt{\varepsilon_0}\frac{\omega}{c}\sin\theta, \tag{5}$$

where ω is the angular frequency, c is the speed of light in free-space, and ε_0 is the optical constant of a prism substrate.

On the other hand, the reflection characteristics for transverse-electric (TE) polarization are determined simply by replacing the expression of Eq. (4) [16] with the Fresnel reflection coefficient, which is given by

$$r_{jk}=\frac{\left(\frac{k_{zj}}{\sqrt{\varepsilon_j\varepsilon_k}}-\frac{k_{zk}}{\sqrt{\varepsilon_j\varepsilon_k}}\right)}{\left(\frac{k_{zj}}{\sqrt{\varepsilon_j\varepsilon_k}}+\frac{k_{zk}}{\sqrt{\varepsilon_j\varepsilon_k}}\right)}. \tag{6}$$

While the use of guided-mode plasmon resonances occurring for oxidized silver films in TE polarization might be an interesting way to extend the dynamic range of an optical biosensor [13], its reflection characteristic with a largely broad resonance curve is not appropriate for SPR imaging detection where sharp absorption resonances are demanded. Thus, in this study, we intend to demonstrate the theoretical investigations only for TM polarization.

Assuming that biomolecular reactions produce a change in the refractive index n_4 of a SAM layer and do not induce a change in its thickness, a variance of the reflectance R occurs with increasing n_4 when the incidence angle is fixed, and therefore the sensitivity of a SPR imaging biosensor is defined as

$$S=\frac{dR}{dn_4}. \tag{7}$$

In order to calculate the sensitivity of Eq. (7), a Lorentzian approximation of the reflectivity derived for the excitation of surface plasmons has been generally used [17,18]. However, since the conventional Lorentzian approximation approach is not simply applicable to our SPR configuration with a six-layer structure [17], the sensitivity S was obtained by differentiating Eq. (7) directly with respect to n_4, and this can be expressed as follows:

$$S = \frac{dR}{dn_4} = \frac{d}{dn_4}\left|\frac{M_{12}}{M_{22}}\right|^2 = \left(\frac{\left(\frac{d}{dn_4}|M_{12}|\right)|M_{22}| - |M_{12}|\left(\frac{d}{dn_4}|M_{22}|\right)}{|M_{22}|^2}\right)2\left|\frac{M_{12}}{M_{22}}\right|. \tag{8}$$

Now, to determine $(d/dn_4)|M_{12}|$ and $(d/dn_4)|M_{22}|$ in Eq. (8), the derivative of matrix M with respect to n_4 is calculated as

$$\begin{aligned}\frac{d}{dn_4}M = \begin{bmatrix}\frac{d}{dn_4}M_{11} & \frac{d}{dn_4}M_{12}\\ \frac{d}{dn_4}M_{21} & \frac{d}{dn_4}M_{22}\end{bmatrix} &= \frac{d}{dn_4}\left(\begin{bmatrix}1 & r_{01}\\ r_{01} & 1\end{bmatrix}\right.\\ &\times\begin{bmatrix}e^{ik_{z1}d_1} & 0\\ 0 & e^{-ik_{z1}d_1}\end{bmatrix}\begin{bmatrix}1 & r_{12}\\ r_{12} & 1\end{bmatrix}\begin{bmatrix}e^{ik_{z2}d_2} & 0\\ 0 & e^{-ik_{z2}d_2}\end{bmatrix}\\ &\times\begin{bmatrix}1 & r_{23}\\ r_{23} & 1\end{bmatrix}\begin{bmatrix}e^{ik_{z3}d_3} & 0\\ 0 & e^{-ik_{z3}d_3}\end{bmatrix}\begin{bmatrix}1 & r_{34}\\ r_{34} & 1\end{bmatrix}\\ &\times\left.\begin{bmatrix}e^{ik_{z4}d_4} & 0\\ 0 & e^{-ik_{z4}d_4}\end{bmatrix}\begin{bmatrix}1 & r_{45}\\ r_{45} & 1\end{bmatrix}\right) = \begin{bmatrix}1 & r_{01}\\ r_{01} & 1\end{bmatrix}\\ &\times\begin{bmatrix}e^{ik_{z1}d_1} & 0\\ 0 & e^{-ik_{z1}d_1}\end{bmatrix}\begin{bmatrix}1 & r_{12}\\ r_{12} & 1\end{bmatrix}\begin{bmatrix}e^{ik_{z2}d_2} & 0\\ 0 & e^{-ik_{z2}d_2}\end{bmatrix}\\ &\times\begin{bmatrix}1 & r_{23}\\ r_{23} & 1\end{bmatrix}\begin{bmatrix}e^{ik_{z3}d_3} & 0\\ 0 & e^{-ik_{z3}d_3}\end{bmatrix}\frac{d}{dn_4}\left(\begin{bmatrix}1 & r_{34}\\ r_{34} & 1\end{bmatrix}\right)\\ &\times\begin{bmatrix}e^{ik_{z4}d_4} & 0\\ 0 & e^{-ik_{z4}d_4}\end{bmatrix}\begin{bmatrix}1 & r_{45}\\ r_{45} & 1\end{bmatrix} + \begin{bmatrix}1 & r_{01}\\ r_{01} & 1\end{bmatrix}\\ &\times\begin{bmatrix}e^{ik_{z1}d_1} & 0\\ 0 & e^{-ik_{z1}d_1}\end{bmatrix}\begin{bmatrix}1 & r_{12}\\ r_{12} & 1\end{bmatrix}\begin{bmatrix}e^{ik_{z2}d_2} & 0\\ 0 & e^{-ik_{z2}d_2}\end{bmatrix}\\ &\times\begin{bmatrix}1 & r_{23}\\ r_{23} & 1\end{bmatrix}\begin{bmatrix}e^{ik_{z3}d_3} & 0\\ 0 & e^{-ik_{z3}d_3}\end{bmatrix}\\ &\times\begin{bmatrix}1 & r_{34}\\ r_{34} & 1\end{bmatrix}\frac{d}{dn_4}\left(\begin{bmatrix}e^{ik_{z4}d_4} & 0\\ 0 & e^{-ik_{z4}d_4}\end{bmatrix}\right)\begin{bmatrix}1 & r_{45}\\ r_{45} & 1\end{bmatrix}\\ &+\begin{bmatrix}1 & r_{01}\\ r_{01} & 1\end{bmatrix}\begin{bmatrix}e^{ik_{z1}d_1} & 0\\ 0 & e^{-ik_{z1}d_1}\end{bmatrix}\begin{bmatrix}1 & r_{12}\\ r_{12} & 1\end{bmatrix}\\ &\times\begin{bmatrix}e^{ik_{z2}d_2} & 0\\ 0 & e^{-ik_{z2}d_2}\end{bmatrix}\begin{bmatrix}1 & r_{23}\\ r_{23} & 1\end{bmatrix}\begin{bmatrix}e^{ik_{z3}d_3} & 0\\ 0 & e^{-ik_{z3}d_3}\end{bmatrix}\\ &\times\begin{bmatrix}1 & r_{34}\\ r_{34} & 1\end{bmatrix}\begin{bmatrix}e^{ik_{z4}d_4} & 0\\ 0 & e^{-ik_{z4}d_4}\end{bmatrix}\frac{d}{dn_4}\left(\begin{bmatrix}1 & r_{45}\\ r_{45} & 1\end{bmatrix}\right).\end{aligned} \tag{9}$$

To compute the differential form of the individual interface matrix I_{jk} and layer matrix L_j, two components of r_{jk} and $e^{ik_{zj}d_j}$ should be differentiated. After substituting Eq. (5) and differentiating r_{jk} with respect to n_4, we obtain a differentiation form of Eq. (4) as

$$\frac{d}{dn_j}(r_{jk}) = -\frac{d}{dn_k}(r_{jk}) = \frac{d}{dn_j}\left(\frac{\frac{k_{zj}}{n_j^2} - \frac{k_{zk}}{\varepsilon_k}}{\frac{k_{zj}}{n_j^2} + \frac{k_{zk}}{\varepsilon_k}}\right) = \frac{\left(\frac{k_{zj}}{n_j^2} - \frac{k_{zk}}{\varepsilon_k}\right)\left(\frac{2k_{zj}}{n_j^3} - \frac{w^2}{c^2 n_j k_{zj}}\right)}{\left(\frac{k_{zj}}{n_j^2} + \frac{k_{zk}}{\varepsilon_k}\right)^2} - \frac{\left(\frac{2k_{zj}}{n_j^3} - \frac{w^2}{c^2 n_j k_{zj}}\right)}{\left(\frac{k_{zj}}{n_j^2} + \frac{k_{zk}}{\varepsilon_k}\right)}. \tag{10}$$

Also, by introducing Eq. (5) in $e^{ik_{zj}d_j}$, the differentiation form of $e^{ik_{zj}d_j}$ with respect to n_4 is obtained as

$$\frac{d}{dn_j}(e^{ik_{zj}d_j}) = \frac{d}{dn_j}(e^{id_j\sqrt{n_j^2(\omega/c)^2 - k_x^2}}) = \frac{id_j w^2 e^{i2k_{zj}d_j}}{c^2 k_{zj}}. \tag{11}$$

Finally, by obtaining $(d/dn_4)|M_{12}|$ and $(d/dn_4)|M_{22}|$ from Eq. (9) and inserting them into Eq. (8), one can calculate the sensitivity S for a target that induces a refractive index change of n_4.

3. RESULTS AND DISCUSSION

A. Effect of Silver Oxidation

Figure 2 shows the characteristics of reflectance R and its sensitivity dR/dn_4 when an initial thickness of the silver film is 40 nm, and the superstrate of a pure water solution surrounds a SAM layer with a refractive index of n_4=1.5. When a homogeneous Ag_2O layer is formed by oxidizing a thin silver film, the oxidation is accompanied by an increment in thickness. Previously, it was reported that the growth of the Ag_2O layer occurs at the expense of the underlying Ag film, and its thickness is approximately equal to 1.5 times that of the converted Ag layer [13]. In Fig. 2(a), the reflectance curves are calculated when the Ag_2O thicknesses are 0, 6, 12, 18, 30, 42, and 60 nm. The resonance angle increases with the Ag_2O thickness in a wide range from 54.7° for no oxidation to more than 85° for thick Ag_2O formation over 30 nm. Also, the reflectivity of a SPR biosensor becomes broader with a growing silver oxide layer because thicker oxide coatings lead to resonant excitations of surface plasmons prompted by photons with a larger incidence angle. These changes in the SPR angle and curve width by silver oxidation are quite consistent with the previous study for partly oxidized silver films [13].

In principle, the sensitivity value corresponds to the slope in the reflectance curve. Hence, the sensitivity at the resonance angle is obtained to be almost zero. As an example, when the Ag_2O thickness is 6 nm, the SPR angle is 57.6°, and its magnitude of sensitivity is determined to be 0.008 in Fig. 2(b), while the positive and negative peak sensitivities are 0.308 at 56.7° and −0.131 at 58.4°. In particular, as the gradient in reflectivity is steeper for incidence conditions preceding the resonance angle, the magnitude of the positive peak is generally larger than that of the negative one. It is found from Fig. 2(b) that the

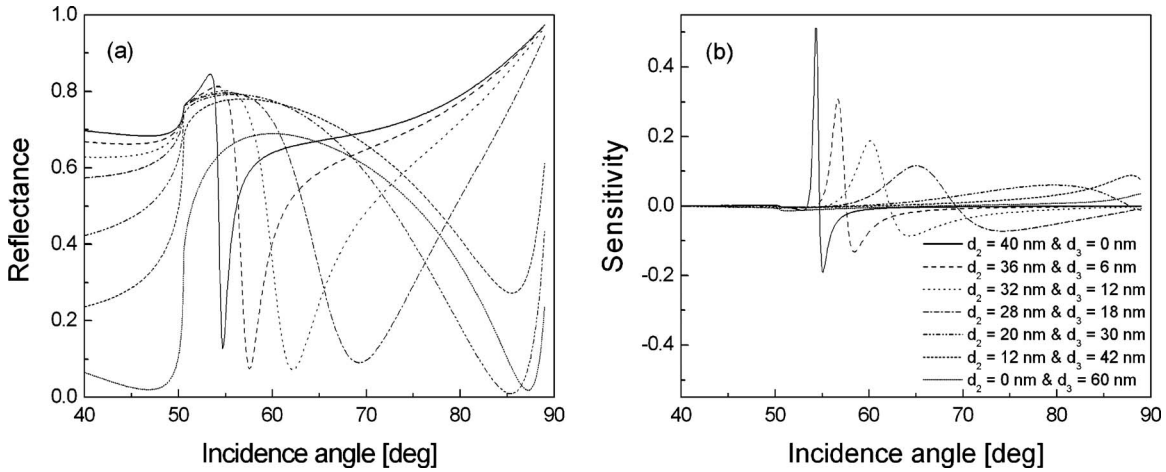

Fig. 2. (a) SPR reflectance R and (b) its sensitivity dR/dn_4 as functions of incidence angle when the growth of silver oxide layer occurs at the expense of the underlying silver film. The initial thickness of silver film is $d_2=40$ nm and $n_4=1.50$.

maximum in sensitivity is decreased with increasing Ag_2O thickness because the oxide layer makes SPR curves broader.

In Fig. 3, the peak values of the sensitivity dR/dn_4 were calculated as a function of the silver film when $n_4=1.33$, i.e., no SAM layer in water. The maximum sensitivity was obtained to be as high as 1.64 at $d_2=60$ nm and $d_3=0$ nm. Similar to the results in Fig. 2(b), Fig. 3 shows a decreasing sensitivity with the thickness of Ag_2O in all cases. Note that an oxidation of silver film occurs along the direction of a solid white arrow implying the thickness ratio of a formation of Ag_2O to a converted silver film. A high sensitivity larger than 1 is observed at a narrow band of $d_3<5$ nm when the silver film thickness is between 45 and 70 nm. Notable reduction in sensitivity is mainly attributed to the plasmon resonance occurring at a higher incidence angle and correspondingly broader and shallower SPR curves. Interestingly, these trends resemble the dramatic change in the SPR signal induced by thin carbon coatings evaporated onto silver films, where

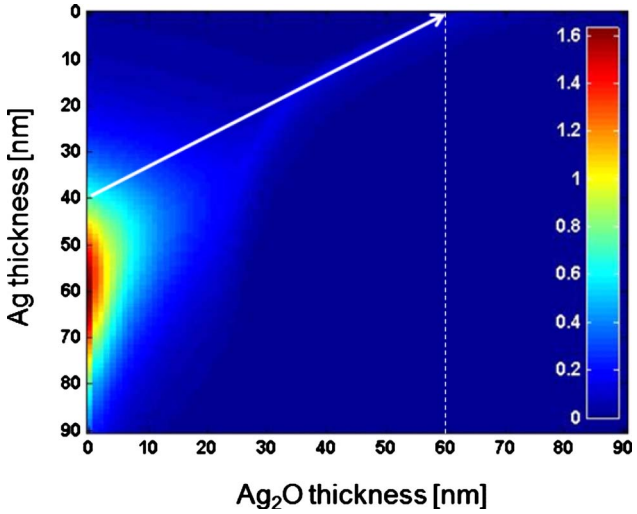

Fig. 3. (Color online) Peak sensitivity of SPR imaging when the thickness of the Ag_2O layer increases. The silver thickness varies from 0 to 90 nm and $n_4=1.33$. The white arrow indicates the oxidation progress of the silver film with an initial thickness of 40 nm.

the strong absorption of the substrate caused a significant degree of plasmon damping [19]. It seems that a similar absorptive damping process associated with Ag_2O formation is responsible for the SPR changes, as the oxide layer possesses a nonzero imaginary dielectric component. This effect is confirmed by calculation data in Fig. 4, demonstrating the deterioration in sensitivity characteristics for silver substrates with the highest sensitivity, i.e., $d_2=60$ nm, caused by the growth of a silver oxide layer. The results present a significant change in the curve angular width (CAW) and minimum reflectance at resonance (MRR) characteristics upon the degree of silver oxidation. Consequently, it should be emphasized that preventing silver oxidation is a crucial concern in an actual fabrication of a silver-film-based SPR imaging biosensor for improving the sensitivity and spatial resolution.

B. Effect of SAM Formation

Also of interest is the influence of biomolecular interactions on the sensitivity of a SPR imaging biosensor. Since SPR characteristics in terms of the resonance angle are changed significantly with an adsorption of target analytes, target dependence is closely linked to the resonance broadening, especially if a significant target refractive index change is involved. As stipulated by the plasmon dispersion relation, the SPR signal is intrinsically nonlinear with the local change in the environments, and achieving high sensitivity becomes therefore complicated due to this nonlinearity and correlated resonance broadening [20]. Figure 5 shows the calculated peak sensitivity, in the case that a biomolecular interaction forms a SAM with respect to the refractive index of $n_4=1.50$ in water solutions. While overall trends are consistent compared to the results in Fig. 3, the sensitivity values are smaller than those of $n_4=1.33$ in most cases.

To confirm this, we calculated SPR curves and sensitivity characteristics for a silver substrate of $d_2=60$ nm and $d_3=0$ nm. Figure 6 shows that the resonance shifts to a higher angle, and the peak sensitivity decreases slightly as n_4 varies from 1.33 to 1.70. Increasing local refractive index change caused by a SAM formation on a metal film leads to a SPR angle shift and contributes to the broadening of the SPR curve, finally resulting in a reduction in

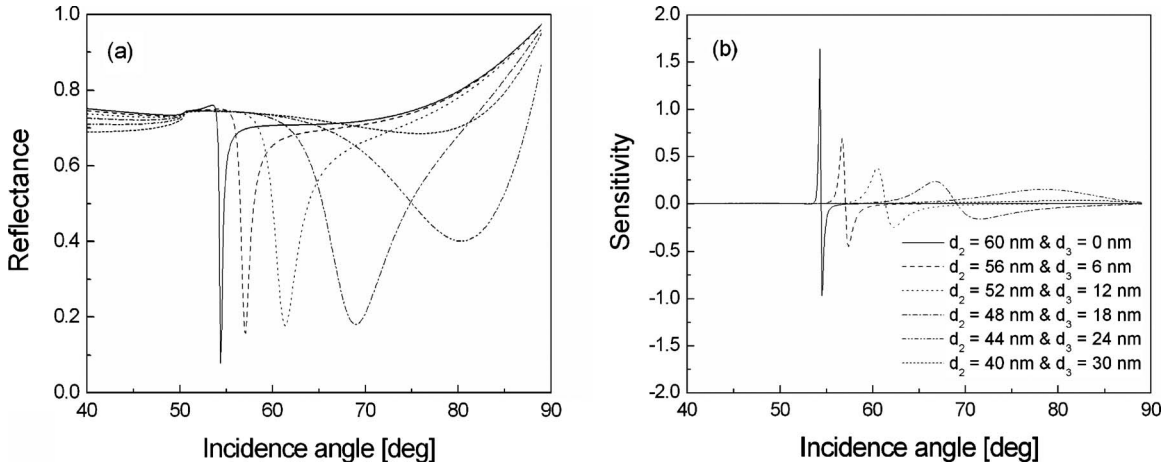

Fig. 4. (a) SPR reflectance and (b) its sensitivity when the thickness of Ag_2O layer increases. The initial thickness of a silver film is 60 nm and n_4=1.33.

the imaging sensitivity. However, as changes in both CAW and MRR are not significant as shown in Fig. 6(a), the peak sensitivity is not more rapidly reduced than for Ag_2O formation in Fig. 4(b). In short, the variation in SPR signals by the SAM formation can be attributed to a broader SPR curve and often degrades the sensitivity of the SPR imaging biosensor.

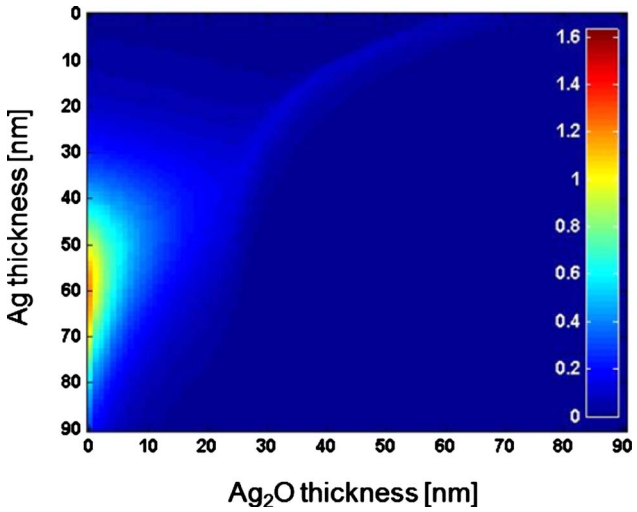

Fig. 5. (Color online) Peak sensitivity of SPR imaging when the thickness of Ag_2O layer increases. The silver thickness varies from 0 to 90 nm and n_4=1.50.

C. Effect of Bimetallic Substrates

In order to surmount the drawbacks of the Ag_2O formation, a bimetallic surface where a thin gold coating is directly deposited over a silver substrate to protect it from oxidation is proposed as an alternative SPR imaging structure. In Fig. 7, the peak sensitivity was obtained as a function of silver and gold film thicknesses. In general, the sensitivity was decreased monotonically when the thickness of gold film is increased. This is because a gold layer with a larger attenuation than silver may cause an inefficient excitation of surface plasmons [2]. Figure 8 illustrates the resonance and sensitivity characteristics calculated for d_2=60 nm. Compared to the SPR structure without an additional gold layer, bimetallic substrates presented a noticeable increment of MRR and consequently lead to a reduced sensitivity for thicker gold thicknesses. It is therefore important to realize an extremely thin gold layer less than $d_{Au}<3$ nm so that the sensitivity obtained from the silver layer would not be degenerated by an introduction of thin gold layers. In terms of practical implementation of a bimetallic substrate, al-

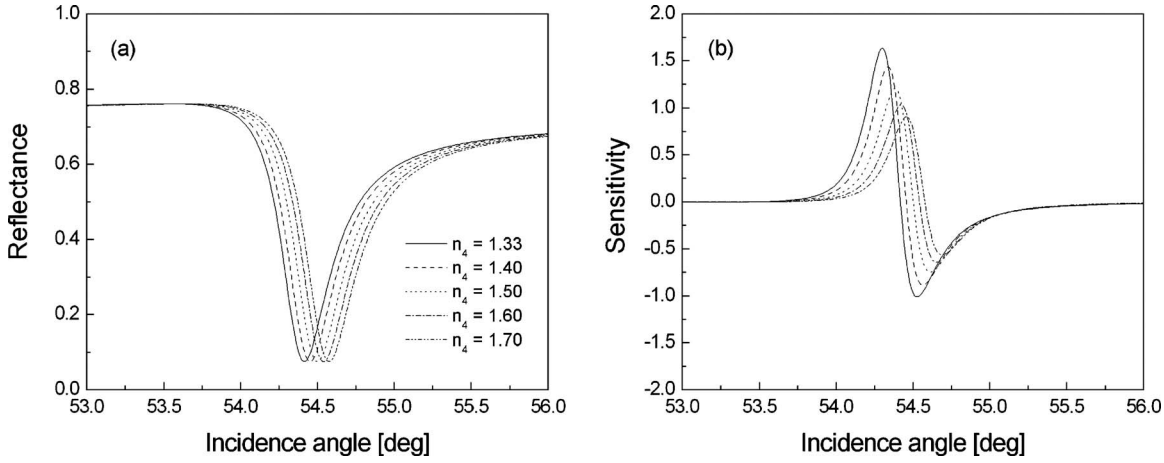

Fig. 6. (a) SPR reflectance and (b) its sensitivity for d_2=60 nm and d_3=0 nm, when n_4 is changed from 1.33 to 1.70.

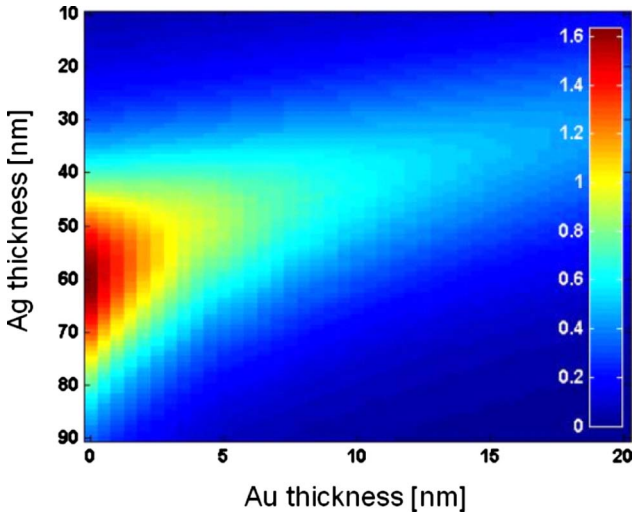

Fig. 7. (Color online) Peak sensitivity of SPR imaging when the thickness of gold layer increases up to 20 nm. Silver film thickness varies from 10 to 90 nm and $n_4=1.33$.

though difficulties in fabrication may increase, ultrathin gold films can be obtained by sputtering a gold target by means of argon and oxygen ion beams [21].

It should be also emphasized that a bimetallic substrate is advantageous in terms of the imaging sensitivity compared to a conventional gold substrate with a high resistance to oxidation. While the results for a thin-gold-film-based SPR imaging biosensor are not shown, when $n_4=1.33$ and $d_4=1$ nm, the peak sensitivity is obtained to be 0.283 at the gold thickness of 56 nm. In Fig. 7, it is shown that the sensitivity of bimetallic Ag/Au substrates exhibits a better performance than for gold substrate at a wide range of Ag and Au thicknesses, implying that the bimetallic substrate can be used as an effective way to achieve a high sensitivity as well as to prevent a silver oxidation.

Moreover, it is intriguing to find in Fig. 7 that, for a silver film thickness ranging from 30 to 40 nm, the bimetallic substrate shows a slight increase in sensitivity, which is contrary to the results of Fig. 8. Also, for 40 nm$\leq d_2 \leq$45 nm, its sensitivity does not change significantly with a gold deposition, and thus when a gold film thickness is larger than 5 nm, bimetallic surfaces showed a better sensitivity than even for $d_2=60$ nm whose initial sensitivity at $d_3=0$ nm was highest. It is attributed to the fact that, for $d_2\leq 45$ nm, the attachment of gold film plays an important role in assisting an efficient excitation of plasmons rather than in absorbing the propagating plasmons supported by the silver film. The results imply an interesting postulation that we may select the silver layer thickness of Ag/Au bimetallic substrates depending on the minimally controllable coating thickness of a gold film. In other words, if the reliable resolution of gold coating in fabrication processes is provided by less than 3 nm, it is desired to achieve a silver thickness of $d_2\approx 60$ nm. If a silver thickness is chosen at around 40 nm, however, an ultrathin gold film is not mandatory, and the performance of bimetallic substrates is less sensitive to fabrication errors in gold thickness, although the maximally achievable sensitivity can be degraded.

Additionally, we considered the effect of the SAM formation on the sensitivity of Ag/Au bimetallic substrates in Fig. 9. As it is expected, the sensitivity of SPR imaging tends to underperform that of the initial condition that $n_4=1.33$ due to a resonance shift and closely related broadening of SPR characteristics. Although the advantage of a gold coating becomes less noteworthy with an increasing refractive index, its important roles of preventing the sensitivity performance from being degraded greatly and of keeping the silver surface unoxidized remain still effective, especially for very thin gold films.

Finally, as an application example of the bimetallic film-based SPR imaging configuration, a binding event of DNA hybridization occurring at the sensor surface is numerically demonstrated. When the refractive index and the effective thickness of a single-stranded DNA are assumed to be $n_4=1.462$ at $\lambda=633$ nm and $d_4=3$ nm [22,23], the maximum sensitivity of a conventional gold-film-based SPR imaging system was obtained to be 0.680 at a gold thickness of 56 nm and an incidence of 58.7°. On the other hand, for Ag/Au bimetallic substrates, the highest sensitivity of 3.059 was achieved when the silver thickness is fixed at 50 nm and gold deposition is not applied, and the peak sensitivity was decreased monotonically with an increasing gold thickness. This trend is identical

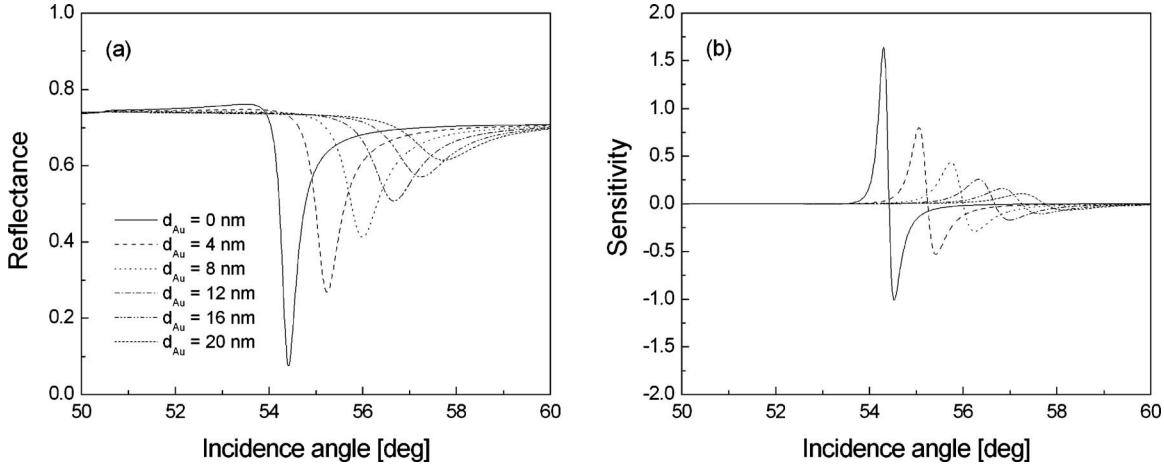

Fig. 8. (a) SPR reflectance and (b) its sensitivity for $d_2=60$ nm and $n_4=1.33$, when the thickness of gold layer increases with a step of 4 nm.

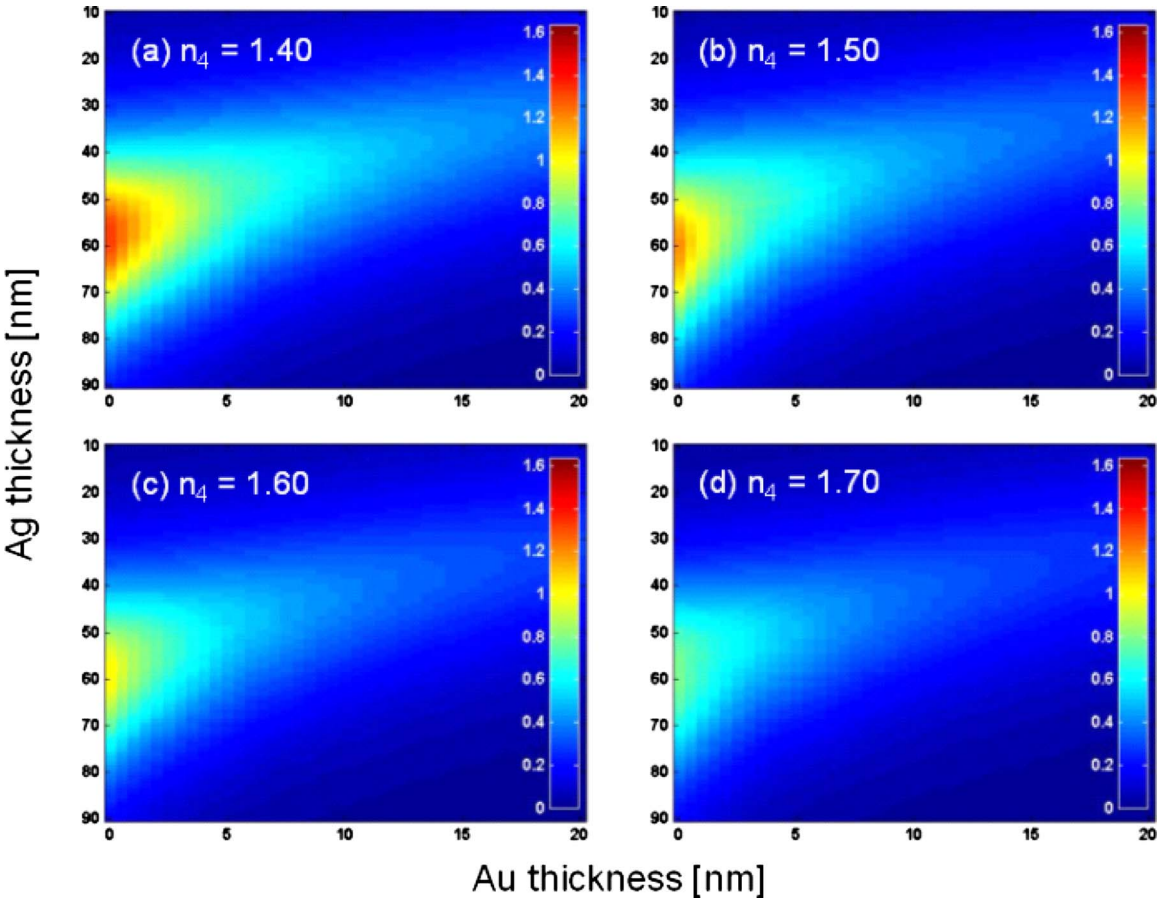

Fig. 9. (Color online) Peak sensitivity of SPR imaging when n_4 is (a) 1.40, (b) 1.50, (c) 1.60, and (d) 1.70. The scale of color bar is the same as that in Fig. 7.

to the results in Figs. 7 and 8. For example, for 5 nm thick gold deposition, which can be reliably obtained by an actual fabrication, the sensitivity was found to have a maximum of 1.980 at an incidence angle of 55.5°, implying 2.9 times better sensitivity.

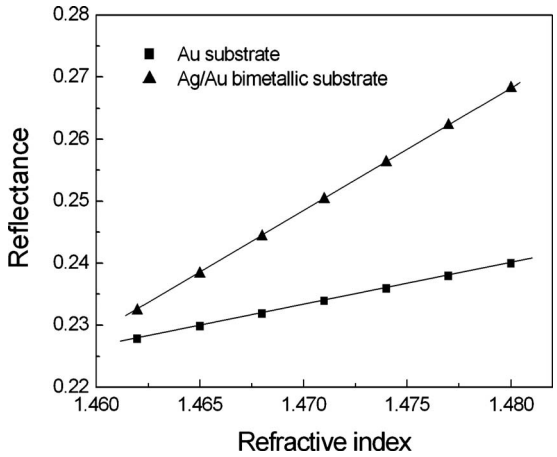

Fig. 10. Linear regression analyses between reflectance and refractive index n_4 for SPR imaging configurations with gold (square) and bimetallic (triangle) substrates. As the refractive index of the dielectric medium surrounding the sensor surface increases from 1.462 to 1.480 in steps of 0.03, the reflectance amplitude increases linearly, and the slope, which implies the sensor sensitivity, of a bimetallic substrate shows about three times better performance than for a gold substrate. The solid lines denote the linear fit of our theoretical results.

In order to graphically demonstrate the sensitivity improvement for bimetallic substrates, a change in reflectance amplitude is calculated when the refractive index n_4 varies from 1.462 (i.e., single-stranded DNA) to 1.480 (i.e., double-stranded DNA) in steps of 0.03. Figure 10 shows that, for a conventional gold substrate, the reflectance increases from 0.228 to 0.240; thus the reflectance change is 0.012, while the reflectance of a SPR imaging system with a bimetallic substrate changes from 0.232 to 0.268, and the net contrast is 0.036. In addition, using the linear regression analyses with a function of $y=Ax+B$, the linear coefficient (A) and the correlation coefficient (R), where R denotes the degree of the linearity, are equal to $A=0.676$ and $R=0.9999$ for a gold substrate and $A=1.992$ and $R=0.9999$ for a bimetallic one. In other words, the shift is completely linear over a wide range of the DNA hybridization reaction, and especially a bimetallic substrate presents about three times greater sensitivity in SPR imaging than a traditional gold substrate.

4. CONCLUSION

In this study, we examined the sensitivity characteristics of a SPR imaging biosensor based on silver substrates. Substantial variations in sensitivity were found among various considerations for silver substrates such as the oxidation process that forms a thin Ag_2O layer on a silver film, a varied refractive index of a SAM layer occurring at

the sensor surface, and an implementation of Ag/Au bimetallic structures to prevent a silver oxidation. First, sensitivity in SPR imaging had a peak value of 1.64 at the silver thickness of 60 nm and tended to be decreased with a growing Ag_2O formation. These trends are associated with an absorptive damping process cause by the Ag_2O layer with a nonzero imaginary optical constant and the correlated changes in CAW and MRR characteristics in SPR curves. Next, the target dependence of the sensitivity suggested that a silver-film-based SPR imaging structure can be designed based on estimated refractive index changes induced by target interactions. More importantly, Ag/Au bimetallic substrates were proposed to avoid undesired oxidation while keeping a good sensitivity of silver films. For very thin gold coatings, bimetallic substrates exhibited a high sensitivity, which is comparable to the result of silver substrates with no protection layer. For a gold deposition of 5 nm, quantitative analyses showed that the SPR signal can be amplified up to three times for Ag/Au substrates, yielding an enhanced sensing performance than the case of a conventional gold substrate. This study demonstrated a significant potential for applying Ag/Au bimetallic substrates to a sensitive SPR imaging detection of various biomolecular interactions.

ACKNOWLEDGMENT

This research was supported by the Kyung Hee University Research Fund in 2009 (KHU-20090720).

REFERENCES

1. B. Rothenhäusler and W. Knoll, "Surface-plasmon microscopy," Nature **332**, 615–617 (1988).
2. J. Homola, S. S. Yee, and G. Gauglitz, "Surface plasmon resonance sensors: review," Sens. Actuators B **54**, 3–15 (1999).
3. K. L. Prime and G. M. Whitesides, "Self-assembled organic monolayers: Model systems for studying adsorption of proteins at surfaces," Science **252**, 1164–1167 (1991).
4. P. Mitchell, "A perspective on protein microarrays," Nat. Biotechnol. **20**, 225–229 (2002).
5. C. L. Wong, H. P. Ho, T. T. Yu, Y. K. Suen, W. W. Y. Chow, S. Y. Wu, W. C. Law, W. Yuan, W. J. Li, S. K. Kong, and C. Lin, "Two-dimensional biosensor arrays based on surface plasmon resonance phase imaging," Appl. Opt. **46**, 2325–2332 (2007).
6. J. Homola, "Present and future of surface plasmon resonance biosensors," Anal. Bioanal. Chem. **377**, 528–539 (2003).
7. W. P. Hu, S.-J. Chen, K.-T. Huang, J. H. Hsu, W. Y. Chen, G. L. Chang, and K.-A. Lai, "A novel ultrahigh-resolution surface plasmon resonance biosensor with an Au nanocluster-embedded dielectric film," Biosens. Bioelectron. **19**, 1465–1471 (2004).
8. K. M. Byun, M. L. Shuler, S. J. Kim, S. J. Yoon, and D. Kim, "Sensitivity enhancement of surface plasmon resonance imaging using periodic metallic nanowires," J. Lightwave Technol. **26**, 1472–1478 (2008).
9. X.-M. Zhu, P.-H. Lin, P. Ao, and L. B. Sorensen, "Surface treatments for surface plasmon resonance biosensors," Sens. Actuators B **84**, 106–112 (2002).
10. M. F. Al-Kuhaili, "Characterization of thin films produced by the thermal evaporation of silver oxide," J. Phys. D: Appl. Phys. **40**, 2847–2853 (2007).
11. H. Sahm, C. Charton, and R. Thielsch, "Oxidation behavior of thin silver films deposited on plastic web characterized by spectroscopic ellipsometry (SE)," Thin Solid Films **455–456**, 819–823 (2004).
12. E. D. Palik, *Handbook of Optical Constants of Solids* (Academic, 1985).
13. H. Libardi and H. P. Grieneisen, "Guided-mode resonance absorption in partly oxidized thin silver films," Thin Solid Films **333**, 82–87 (1998).
14. S. Park, G. Lee, S. H. Song, C. H. Oh, and P. S. Kim, "Resonant coupling of surface plasmons to radiation modes by use of dielectric gratings," Opt. Lett. **28**, 1870–1872 (2003).
15. A. Yariv and P. Yeh, *Optical Waves in Crystals: Propagation and Control of Laser Radiation* (Wiley, 1984).
16. A. Shalabney and I. Abdulhalim, "Electromagnetic fields distribution in multilayer thin film structures and the origin of sensitivity enhancement in surface plasmon resonance sensors," Sens. Actuators, A **159**, 24–32 (2010).
17. H. Raether, *Surface-Plasmons on Smooth and Rough Surfaces and on Gratings* (Springer-Verlag, 1988).
18. M. Piliarik and J. Homola, "Surface plasmon resonance (SPR) sensors: approaching their limits?" Opt. Express **17**, 16505–16517 (2009).
19. I. Pockrand, "Surface plasma oscillations at silver surfaces with thin transparent and absorbing coatings," Surf. Sci. **72**, 577–588 (1978).
20. S. J. Yoon and D. Kim, "Target dependence of the sensitivity in periodic nanowire-based localized surface plasmon resonance biosensors," J. Opt. Soc. Am. A **25**, 725–735 (2008).
21. A. I. Stognij, N. N. Novitskii, S. D. Tushina, and S. V. Kalinnikov, "Preparation of ultrathin gold films by oxygen-ion sputtering and their optical properties," Tech. Phys. **48**, 745–748 (2003).
22. D. E. Gray, S. C. Case-Green, T. S. Fell, P. J. Dobson, and E. M. Southern, "Ellipsometric and interferometric characterization of DNA probes immobilized on a combinatorial array," Langmuir **13**, 2833–2842 (1997).
23. S. Elhadj, G. Singh, and R. F. Saraf, "Optical properties of an immobilized DNA monolayer from 255 to 700 nm," Langmuir **20**, 5539–5543 (2004).